ASME/JSME Thermal Engineering Proceedings
Volume 5 — ASME 1991

TRAJECTORIES OF HORIZONTAL BUOYANT FREE JET FLAMES

J. P. Gore and C. Q. Jian
Department of Mechanical Engineering
University of Maryland
College Park, Maryland

ABSTRACT

An experimental and a theoretical study of horizontal jet flames burning methane in room air is reported. Measurements of mean flame trajectories using video photography and image analysis are reported for three turbulent diffusion flames. The measurements are used to evaluate a numerical analysis based on an adaptive curvilinear coordinate system. The laminar flamelet concept is used in conjunction with a dual (momentum and buoyancy) mixing length turbulence model. Predictions of mean flame trajectories are in good agreement with measurements. New data concerning the intermittency of the flame surface are obtained. These show very high visible flame surface intermittency, compared to similar vertical flames, suggesting strong effects of buoyancy on turbulent mixing.

INTRODUCTION

Horizontal (normal to the direction of gravity) jet flames under normal gravity occur in fires resulting from fuel pipe leaks and oil and gas well diverters. Many furnaces utilize horizontal flames as well. When the surroundings are stagnant, the horizontal jet flames turn progressively away from the injector axis due to the action of buoyancy until a predominantly vertical flow is obtained. Due to the practical applications, a procedure for calculating the structure and radiation properties of horizontal jet flames is needed.

In addition to the global effect of turning the flow in a direction opposite to the gravity vector, buoyancy produces turbulent velocities in the presence of temperature gradients and fluctuations. In a horizontal jet flame, the density decreases in the direction of gravity in the upper half leading to instability and production of turbulence (Lamb, 1946). In the lower half, the density increases in the direction of gravity contributing to the suppression of turbulence. Such behavior is termed "lofting" in the atmospheric sciences (Pasquill and Smith, 1983)

Due to the complexity of the processes described above, to our knowledge only two studies of horizontal jet flames have been reported in the literature. Becker et al.(1980) have reported dimensional analysis of horizontal jet flames. These authors relate the dimensions of this flame to those of a vertical jet flame. They observe that this is logical since in the low and the high initial momentum limits, the configuration degenerates into a vertical buoyant plume and a vertical forced jet respectively. Thus the burner exit Richardson number (Ri_L) defined in eq. (1) and the length of a corresponding vertical flame (L_o) are used to obtain the parameters controlling the overall geometry.

$$Ri_L = \pi\, a\, \rho_\infty\, L_o^3/4G_o \qquad (1)$$

where a is the acceleration due to gravity and G_o is the momentum flux at the jet exit.

Becker et al. (1981) found that mean shapes of several flames burning a variety of fuels could be correlated using these two parameters as:

$$Y/L_o = f(\xi_L,\ X/L_o) \qquad (2)$$

where ξ_L is the dimensionless flame length defined as $\xi_L = Ri_L^{(1/3)}$.
Y and X are the vertical and horizontal spread of the visible flame defined in Fig. 1 for reference.

For calculation of thermal radiation from flames, scalar property distributions must be known together with estimates of their fluctuations in addition to global flame shape and size that may be obtained from highly

engineered correlations (Faeth et al., 1989). Therefore, further investigation of the problem is essential.

Gosman et al. (1977) made an early attempt at calculating the mean distributions of such properties in horizontal jet flames using a k-ε-g turbulence model. A marching procedure was used in the horizontal direction considering diffusion in only two cross stream directions. Diffusion in the horizontal direction becomes significant as the jet turns under the action of buoyancy. The authors restricted their calculations and comparison to the nearly horizontal region of the flame and expanded the grid as the jet spread and turned slightly. Measurements of mean temperatures and oxygen concentrations were used to evaluate the analysis. The spread rates of the jet flame were under-predicted considerably particularly at farther axial locations. This may be due to an inadequate treatment of buoyancy generated turbulence. The calculations were terminated at relatively short distance from the injector exit due to large increase in computational grid caused by expansion and turning of the jet.

In analysis of flows of power plant effluent water into bays, Madni and Pletcher (1977) utilized an adaptive grid to control the expansion of the computational domain caused by the turning of the jet. The jet was assumed to remain symmetric around the axial curvilinear coordinate allowing consideration of diffusion only in the radial direction. Due to small density gradients, Boussinesq approximations were used. The jet turned at a much lower rate than a low momentum horizontal flame. A mixing length model of turbulence together with a modification due to buoyancy similar to the one suggested in the atmospheric turbulence literature (see for example Pasquil and Smith, 1983) was used. However, the constant (K_4) involved in the contribution of buoyancy to turbulence was changed from 18 to 1 in order to obtain reasonable predictions of the jet trajectories.

In the past fifteen years, significant progress has been made in turbulence modelling using the second moment closure schemes (Launder, 1985, Chen and Singh, 1990) including treatment of the body forces and streamline curvature (Launder, 1985; Chen and Singh, 1986). However, much of this work has been in nonreacting vertical jets and plumes. Second moment closure schemes have also been applied to vertical buoyant flames (Jeng and Faeth, 1984; Tamanini, 1977). However, perhaps due to the difficulties posed by high intermittency and streamline curvature observed in horizontal jet flames, second moment closure schemes have not been applied in the past. Recent work in nonreacting horizontal buoyant jets has also utilized the mixing length turbulence model (Sinclair et al., 1990).

In the present work, horizontal jet flames with three exit Reynolds numbers were visualized to observe mean flame shapes and trajectories. These were compared with the correlation of Becker et al. (1980). A variable density version of the adaptive grid procedure of Madni and Pletcher (1977) was developed. Consistent with the status of turbulence modelling briefly described above, a mixing length model of turbulent diffusivity together with a buoyancy correction was used. The two constants of this model were calibrated using one of the present flames. The predictions of mean jet trajectories are compared with measurements. New data concerning intermittency of the visible flame surface are reported highlighting the importance of buoyancy generated turbulence.

EXPERIMENTAL METHODS

The burner is made from a 6 mm diameter 250 mm long stainless steel tube with a wire screen flow straightner at the inlet. Methane gas from commercial cylinders is metered using a calibrated rotameter. Three operating conditions are selected as representative (of twelve studied to date) for the present discussion. These are summarized in Table 1. The flames were surrounded by a fine wire screen enclosure. The exhaust hood was traversed to a suitable axial position for the different operating conditions. In order to avoid the effects of its suction on the flame trajectories, the exhaust fan was shut off 2 minutes prior to making a 30 second 35 frames per second video of all flames. Effects of buildup of exhaust gases in the room during the 2.5 minute period were minimal due to its size (6 m x 6 m x 2.5 m).

TABLE 1 SUMMARY OF FLAMES STUDIED

Reynolds Number	4300	6500	12500
Fuel Flow Rate mg/s	229	346	665
Heat Release Rate kW (estimated)	12	18.2	35
Vertical Flame Length (Visible) L_o , mm	737	838	1242
Jet Exit Momentum Nx1000	2.65	6.06	22.4
Richardson Number Parameter ξ_L	12	10.5	8.9

In order to compare the present flames with the correlations of Becker et al. (1980), corresponding vertical jet diffusion flames were also studied. The length of the vertical flame L_o has been used as a parameter. The measurements of L_o for the present flames are listed in Table 1. The momentum at the injector exit G_o as well as ξ_L the Richardson number parameter used in the correlation of flame size are also noted.

The flame with an exit Reynolds number of 4300 attached naturally at the burner exit while the two with the higher Reynolds numbers were detached (similar to lifted flames in the vertical jet diffusion configuration) from the burner exit. In order to study the baseline case, special pilot flames were not used in the tests described here. However, a pilot flame is now being utilized for consistency with the theoretical model.

The 900 images of each flame were scanned and 30 representative images were selected at random for digitization. Average flame shapes, length and width, mean and fluctuating flame surface intermittency were calculated using the digital images. Measurements using a high speed (1000 Hz) shutter are currently in progress for the three horizontal flames described here as well as their vertical counterparts.

THEORETICAL METHODS

The analysis described in the following is mainly intended to calculate the mean flow properties of the horizontal flames. The turbulent fluctuations in this configuration are very complex due to buoyancy induced instabilities. The mean flow calculations must first define approximate geometric and global properties of the field in which the fluctuating quantities can be calculated. The treatment discussed in the following was used by Madni and Pletcher (1977) for hot water jets issuing into cold water surroundings under the Boussinesq approximations. In the present work, due to the large density gradients in the flow field, the Boussinesq approximation is not made and a variable density calculation is performed.

The governing conservation equations of mass, momentum and mixture fraction are first transformed into an adaptive curvilinear coordinate system. This coordinate system tracks the centerline of the flame as it turns under the action of gravity. In the new coordinate system following assumptions are made: low Mach number, axisymmetric boundary layer flow with no swirl; equal exchange coefficients for all species and heat; the effect of radiation from the flame is the loss of a fixed (constant over the entire flame) fraction of chemical energy release; mixing length model for the jet flow with effects of buoyancy turbulence interactions addressed using a buoyancy correction. The similarity of the flame dimensions normalized by the vertical jet dimensions found by Becker et al. (1980) suggests that the axisymmetric boundary layer assumption in the new coordinate system may be a reasonable first step. The second assumption has been widely used in vertical flame calculations. For the present nonluminous (methane) flames, the third assumption is justified by past performance. The jet flow in the absence of buoyancy is self similar justifying the mixing length approximation. The treatment of buoyancy turbulence interactions with a modified mixing length has been widely used (Madni and Pletcher, 1977; Pasquill and Smith, 1983; and Sinclair et al., 1990). However, it is widely known that this approach neglects the multiscale aspects of turbulence and is to be treated only as a necessary first step.

The curvilinear cylindrical coordinate system is shown in Fig. 1. This consists of

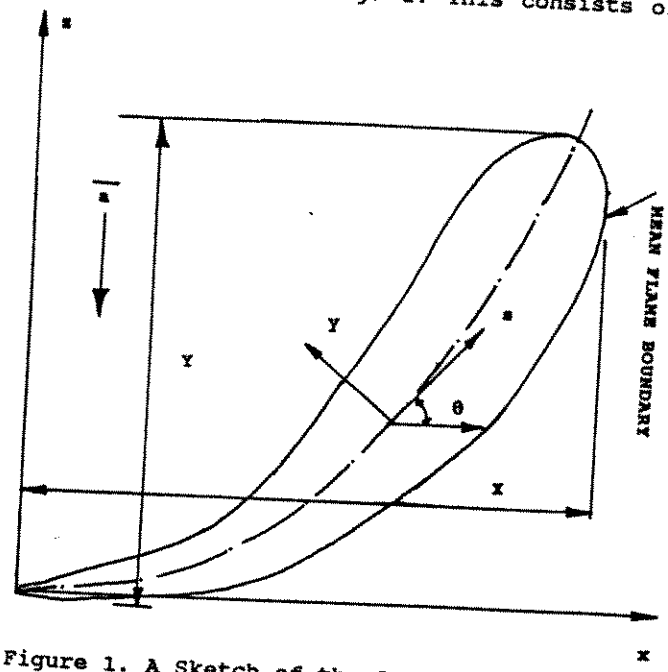

Figure 1. A Sketch of the Coordinate System.

the directions s, Y and the angular coordinate Φ. The original cartesian coordinates x and z are shown for reference. The s coordinate tracks the axis of the jet flame, the Y coordinate is perpendicular to s at each location. Under the assumption of axisymmetric flow (all quantities are invariant in the Φ direction) in the transformed coordinate system, consideration of only Y and s directions is adequate. The gravitational acceleration is represented by a in Fig. 1. Following Madni and Pletcher (1977), the conservation equations for mean mass, mean momentum in the s and y directions and mean mixture fraction are written as follows:

Conservation of Mass:

$$\frac{1}{1-e}\frac{\partial(\rho u)}{\partial s}+\frac{1}{y}\frac{\partial(y\rho v)}{\partial y}-\frac{e\rho v}{(1-e)y}=0 \qquad (3)$$

Conservation of Momentum in s direction:

$$\frac{\rho u}{1-e}\frac{\partial u}{\partial s}+\rho v\frac{\partial u}{\partial y}=(\rho_\infty-\rho)a\sin\theta$$

$$+\frac{1}{(1-e)y}\left(\frac{\partial}{\partial y}\left(y\mu_t(1-e)\right)\frac{\partial u}{\partial y}\right) \qquad (4)$$

Conservation of momentum in the y direction: (written with the turning angle θ as the dependent variable)

$$\left(u^2-\frac{vy}{2}\frac{\partial v}{\partial y}\right)\frac{d\theta}{ds}=\frac{\rho_\infty-\rho}{\rho}a\cos\theta \qquad (5)$$

Mean Mixture Fraction (defined as mass of the local fluid originating in the fuel jet)

$$\frac{\rho u}{1-e}\frac{\partial f}{\partial s}+\rho v\frac{\partial f}{\partial y}=\frac{1}{(1-e)y}\frac{\partial}{\partial y}\left(\frac{y\mu_t}{(1-e)\sigma_f}\frac{\partial f}{\partial y}\right) \quad (6)$$

where e is a local variable related to the coordinate transformation defined as:

$$e=y\frac{d\theta}{ds}\sin\phi \quad (7)$$

It is noted that the density ρ in eqs. (3) - (8) is time averaged while the axial velocity u, the radial velocity v, the mixture fraction f are Favre averaged. Note that the y momentum equation is integrated with respect to ϕ under the assumption of axisymmetry to obtain eq. (5). The turning angle θ is a geometric parameter whose rate of change is defined by the Favre averaged axial velocity, the time averaged local density and the current value of θ. Similar to the radial momentum equation, the remaining conservation equations are integrated with respect to ϕ in order to eliminate the angular dependence following the procedure of Madni and Pletcher (1977).

The time averaged density at each point in the jet is uniquely related to the mean mixture fraction using the state relationships for natural gas (predominantly methane) of Gore (1986). This is an approximate use of the laminar flamelet concept described by Bilger(1977). The approximation is valid for linear variation of the density with mixture fraction in the range of local mixture fraction fluctuations. The approximation is consistent with the present turbulence model. Moreover, Kounalakis et al. (1989) have found that the use of mean mixture fraction in conjunction with state relationships provides better estimates of scalar properties

Turbulence Model

As discussed above the turbulent diffusivity μ_t appearing in the s momentum and the mean mixture fraction equations is obtained using the mixing length model corrected for effects of buoyancy.

$$\mu_t=\rho\frac{l_m^2}{\phi_M^2}\left|\frac{\partial u}{\partial y}\right| \quad (8)$$

where l_m is the mixing length and ϕ_M is the modification to the mixing length due to buoyancy-turbulence interactions. The mixing length is specified as $l_m = K_3\, y_{1/2}\,(U_{max} - U_{min})$. Where K_3 is the turbulence constant, $y_{1/2}$ is the width of the jet at 1/2 velocity point and U_{max} and U_{min} are the maximum and minimum velocities at the local axial station. The recommended value of the constant K_3 for circular jets is 0.0256 (Schlichting, 1979), Madni and Pletcher (1977) used a K_3 of 0.0246. For the present test flames, K_3 was tuned for the forced jet limit and found to be 0.037. Perhaps by coincidence, this is the exactly the value of K_3 recommended by Schlichting (1979) for plane jets and used by James and Edwards (1977) for their plane jet diffusion flames. The reasons for the higher value of K_3 are presently unknown.

The buoyancy induced modification in the mixing length ϕ_M is defined in terms of the gradient Richardson number Ri as follows:

$$\phi_M=(1-K_4 Ri\cos\theta)^{0.25} \quad (9)$$

where the gradient Richardson number Ri is defined as:

$$Ri=aT_\infty\frac{\partial T}{\partial y}/\left(\frac{\partial u}{\partial y}\right)^2 \quad (10)$$

Following Madni and Pletcher (1977), the gradients of velocity and temperature in eq. (10) were approximated based on the centerline and the edge value of the variables. A recent study (Sinclair et al. 1990) of hot water jets in cold water has used the local gradients in the calculation of Ri.

Several values of the constant K_4 have been recommended in the literature. Sinclair et al. (1990) state that this constant should be between 15 and 28; Madni and Pletcher (1977) quote Keyps formula from Bradshaw (1969) to state that the constant K_4 should have a value of 18. They used a value of approximately 16 to obtain the best fit to several measurements of hot water plumes in cold water. In order to match the flame trajectories, a K_4 of 44.1 was used in the present study. Thus it is noted that the turbulence constants for the simple mixing length model are far from universal. A lack of understanding of buoyancy-turbulence interactions is the basic cause of this problem.

Numerical Integration

The equations for conservation of mass, mean axial momentum, mean turning angle, mean mixture fractions described above are solved using an explicit DuFort-Frankel scheme similar to Madni(1975). Madni (1975) used the Boussinesq approximations to include variable density effects only in the body force terms. In the present work, modifications to the finite difference formulation of Madni (1975) were completed to accommodate variable density effects in the convection and diffusion terms in addition to the body force terms. In order to check the present formulation and computer program, constant density flows and hot water in cold water flows of Madni (1975) were computed and found to be in excellent agreement.

In the following, the measurements and predictions of mean flame trajectories and shapes are discussed. The measurements of intermittencies of the visible flame surface for the three flames
are then presented.

RESULTS AND DISCUSSION

Mean Flame Shapes: The maximum visible

spread lengths X in the horizontal direction and Y in the vertical direction (see Fig. 1) normalized by the vertical flame length L_o (listed in Table 1) are plotted as a function of the Richardson number parameter ξ_L in Fig. 2. The data and correlation of Becker et. al.

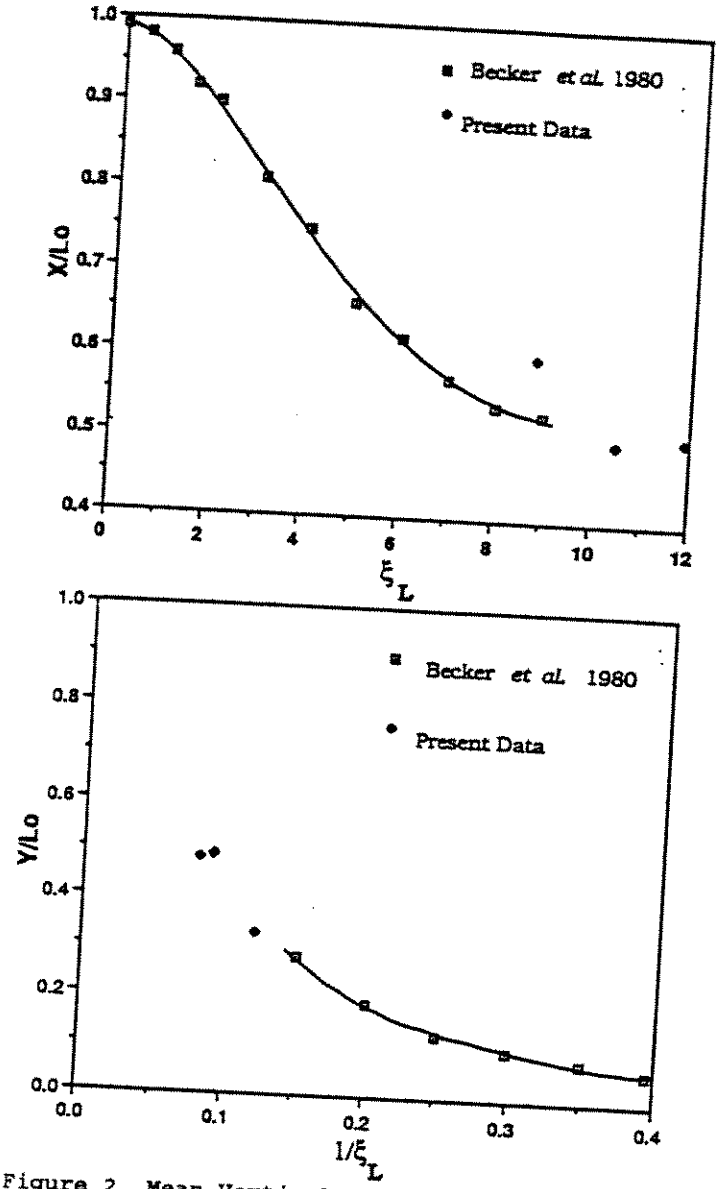

Figure 2. Mean Vertical and Horizontal Spread of Horizontal Jet Flames.

(1980) are also shown for reference. The present operating conditions extend the range of the data covered by Becker et al. (1980). The present Re= 12500 flame is in the transition region between buoyancy and momentum dominated extremes. The other two flames are in the buoyancy dominated region based on the correlation of Becker et al. (1980). However, the present data show somewhat more pronounced effects of momentum. For example, the horizontal length X/L_o for the Re= 12500 is approximately 0.6 instead of 0.5 as predicted by the correlation of previous data. The plateau of X/L_o reached at high values of ξ_L is however similar to that shown by earlier data. The vertical length Y_L also plotted in Fig. 2 as a function of $1/\xi_L$ is in better agreement with the correlation of Becker et al. (1980). However, this choice of the abscissa tends to mask the differences. Discrepancies in flame length and size parameters of the order seen in Fig. 2 can result from the differences in initial conditions of the flames, exposure time and film development method etc., and are expected.

Measurements and predictions of the flame trajectories for the three flames are plotted in Fig. 3. The vertical location of the curvilinear axis of symmetry was determined from the 30 digitized images plotted as a function of horizontal distance from the injector exit. Both lengths are normalized by the injector diameter d. The predictions of

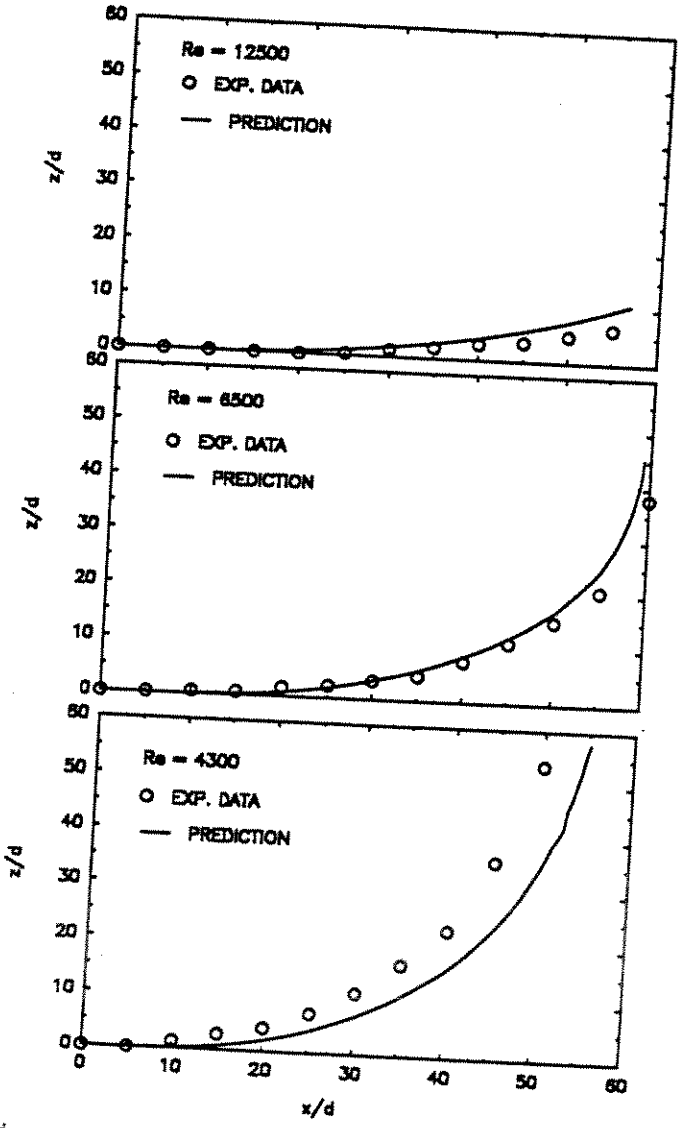

Figure 3. Measurements and Predictions of Mean Jet Trajectories.

the location of the axis of symmetry based on the finite difference analysis described earlier are shown as solid lines.

The Re=4300 flame has the lowest momentum at the jet exit and is attached to the burner. It shows the maximum curvature and rises about 50 diameters in a downstream distance of 50 diameters. The analysis generally underpredicts the curvature by between 10-20 %. The Re=6500 flame with somewhat higher exit momentum rises about 20 diameters at 50 diameters downstream. The trend with the Reynolds number is captured well by the analysis in this range. As the jet exit momentum is increased further (Re=12500), the flame axis lifts only 5 diameters at 50 diameters downstream. Again the present analysis represents the change from buoyancy to transition regime very well. The numerical predictions of maximum spread also show similar agreement with the measurements.

Since the present analysis predicts the mean shapes reasonably well, the experimental data concerning transient flame shapes are studied further. Future analysis will be aimed at predicting fluctuations in various quantities.

Transient Flame Shapes:

Out of the 900 images of each of the three flames captured in the present study, six typical images are sketched in Figs. 4-6. Figure 4 shows the typical flame shapes for the Re=4300 flame. This flame is attached at the injector exit and turns upwards to almost a 45° effective trajectory. The overall appearance of the six images is similar. Generally, the lower interface is less contorted as compared to the upper interface due to the instability of the latter. Occasional breakoff of flame pockets is observed in some of the images. The dashed lines in the sketches shows the blue (no soot) interface while the solid line shows the yellow (soot) interface. As seen from several of the images, soot formation occurs in the upper half of the flame while the lower half remains relatively blue.

Figure 5 shows six representative images for the Re=6500 flame. At this condition, the flame is detached from the injector (which is shown for reference). The flame shapes show a much larger variety with the flame occasionally breaking off into three large pieces. The upper interface is consistently

Figure 4. Representative Instantaneous Flame Shapes, Re =4300.

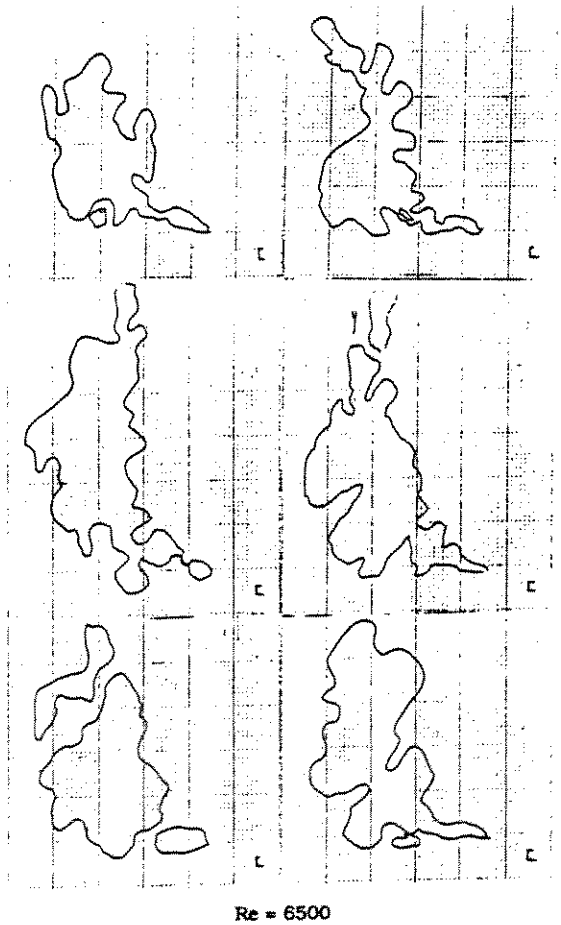

Figure 5. Representative Instantaneous Flame Shapes, Re =6500.

contorted with large penetration of the ambient air into the flame and vice versa. The lower interface is occasionally smooth and generally shows less penetration of ambient air.

The highest Re flame (Re=12500) shows the largest variety of flame shapes as seen in Fig. 6. The flame is generally broken into many pieces with ambient gas often penetrating across the width of the jet. A blue zone as denoted by the dashed lines is observed in all images near the exit perhaps due to premixing with ambient gas in the detached portion of the jet. The flames appear remarkably different than their vertical flame counterparts. The vertical flames show fragmentation only near the flame tip , and even there, to a lesser degree than that shown by the horizontal jets.

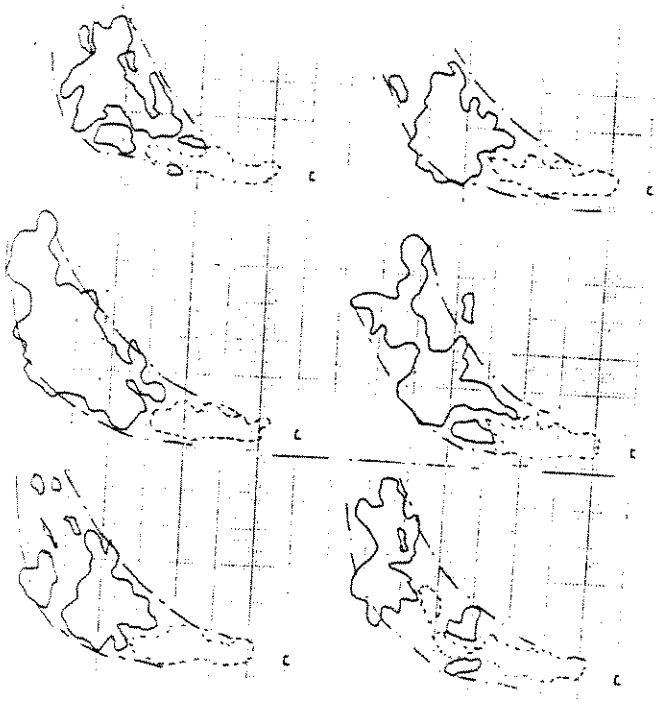

Re = 12500

Figure 6. Representative Instantaneous Flame Shapes, Re =12500.

The observed visible interfaces of the three flames were quantified by using thirty digitized images. The visible flame intermittency at a location (x,z) shown in Fig. 7 is defined as: $I = 1$, if the image is yellow due to soot luminosity at x, z and $I = 0$, if the image is not yellow (has background color) at x, z. Once the data from all thirty images are obtained, the average (over thirty realizations) intermittency of flames is calculated. The mean square intermittency, I'^2 at x,z is calculated from the 30 data sets and the average intermittency. The average intermittency represents the probability of finding the flame at a given location while

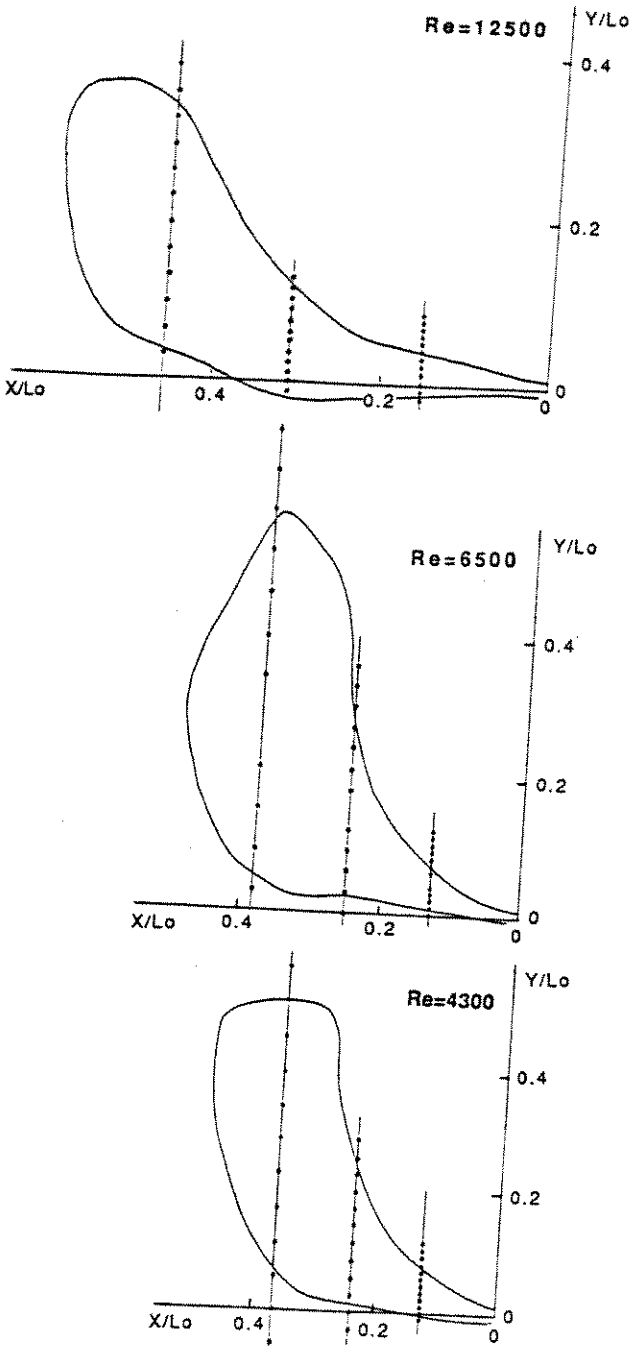

Figure 7. Mean Flame Shapes and Locations for Flame Intermittency Measurements.

the mean square intermittency represents the flame fluctuations due to turbulence.

In the following, average and mean square intermittency at the locations marked by vertical lines (with points on them) in Fig. 7 are discussed. Three downstream locations are selected for each flame. The first location is relatively near the injector exit and all three flames are almost horizontal at this location. The second location is at the

beginning of the turn in the mean flame. The third location is towards the completion of the turn for the two lower Re flames and at an intermediate position for the Re=12500 flame.

Flame Fluctuations: The probability of finding a visible flame (I) at various radial positions at three different downstream locations in the Re=4300 flame is shown in Fig. 8. The horizontal distance from the injector exit x is normalized by Hf which is the mean distance to which the visible flame progresses in the horizontal direction (termed X previously for comparison with Becker et al., 1980). The vertical distance r is measured from the centerline of the injector and is normalized by the local mean visible width Wf of the flame.

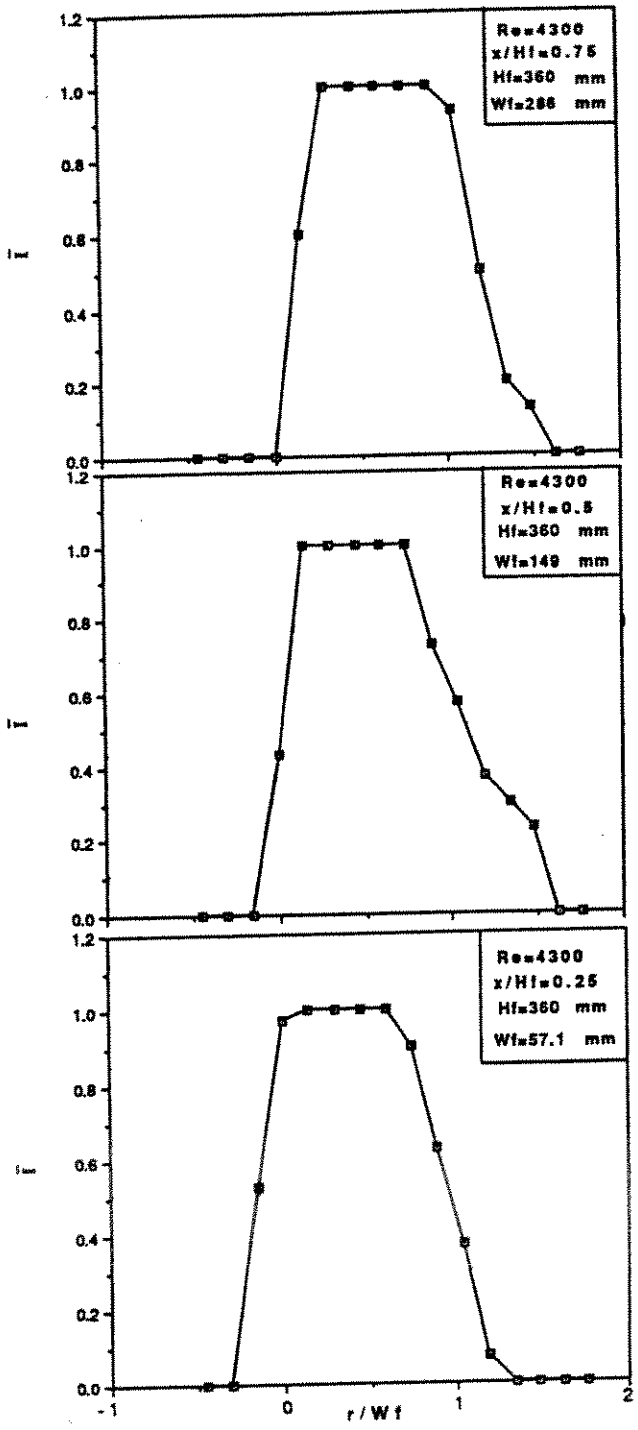

Figure 8. Mean Visible Flame Intermittency, Re = 4300.

In Fig. 8, at the lower interface, the mean intermittency grows very sharply to 1 and retains that value for several points across the flame. In contrast, the intermittency at the upper interface decreases much more slowly. This is a result of the action of buoyancy disturbing the upper flame surface and sending little flamelets out to larger radial locations. At x/Hf= 0.5 position, the slope of the intermittency curve for the upper interface decreases at a fixed radial location. This is due to flame protrusions from a downstream position. The width of the visible flame increases considerably from r/Wf =0.25 to r/Wf=0.75. However, the spread of the flame intermittency appears to scale with the mean width. The lower surface of the flame appears to have very little disturbances even at the downstream positions suggesting that buoyant instability at the upper edge is the cause of flame intermittency.

Figure 9 shows the probability of finding a visible flame at comparable locations in the Re=6500 flame. Due to the higher momentum and turbulence intensity at the jet exit, the mean intermittency profile is almost symmetric for the x/Hf=0.25 position. Near the center of the flame, a region with a mean intermittency of 1 still persists. At the downstream positions, the region of unity mean intermittency shrinks considerably due to buoyancy induced mixing. At the intermediate position (x/Hf=0.5), a second peak is observed in the mean intermittency. This is due to the flames from a downstream location appearing at a specific radial distance above the local mean flame edge. At the position farthest from the injector, the mean intermittency does approach 1 at the axis. However, it decreases symmetrically with radius, since the jet is almost vertical at this position.

The mean intermittency profiles for the Re=12500 flame are shown in Fig. 10. At the position near the injector exit, the lower flame surface appears sharp while the upper flame surface has a larger slope. The probability of finding a visible flame is restricted to a relatively narrow region due to the higher momentum of this jet. As the flame begins to turn under the action of buoyancy, intermittent structures are seen. The intermittency profile at x/Hf=0.5 shows two peaks due to flame protrusions from a downstream location. The distribution appears almost symmetric at the farthest position (x/Hf =0.75) even though the flame is not vertical at this location. The shear generated turbulent fluctuations reach a peak at the downstream locations and probably result in the symmetry.

In Figs. 11-13, the mean square

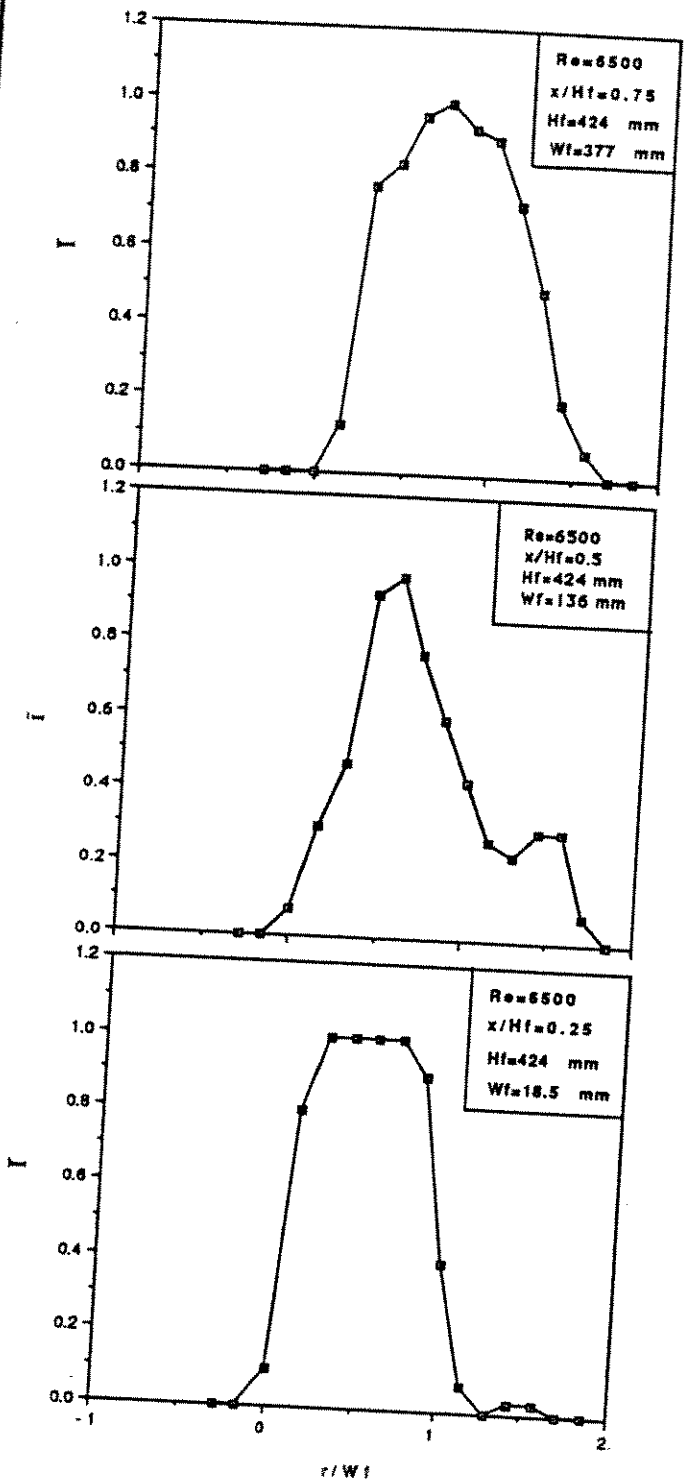

Figure 9. Mean Visible Flame Intermittency, Re = 6500.

intermittency for the three flames is plotted for positions identical to those seen in Figs. 7-10. Figure 11 shows the mean square intermittency for the Re = 4300 flame. The mean square intermittency of an on/off property such as I takes a fundamental value of 0.25 at I = 0.5. This is observed at all positions in Fig. 11. The lower interface consistently shows very narrow distribution of the mean square intermittency while the upper interface shows considerable broadening due to buoyancy.

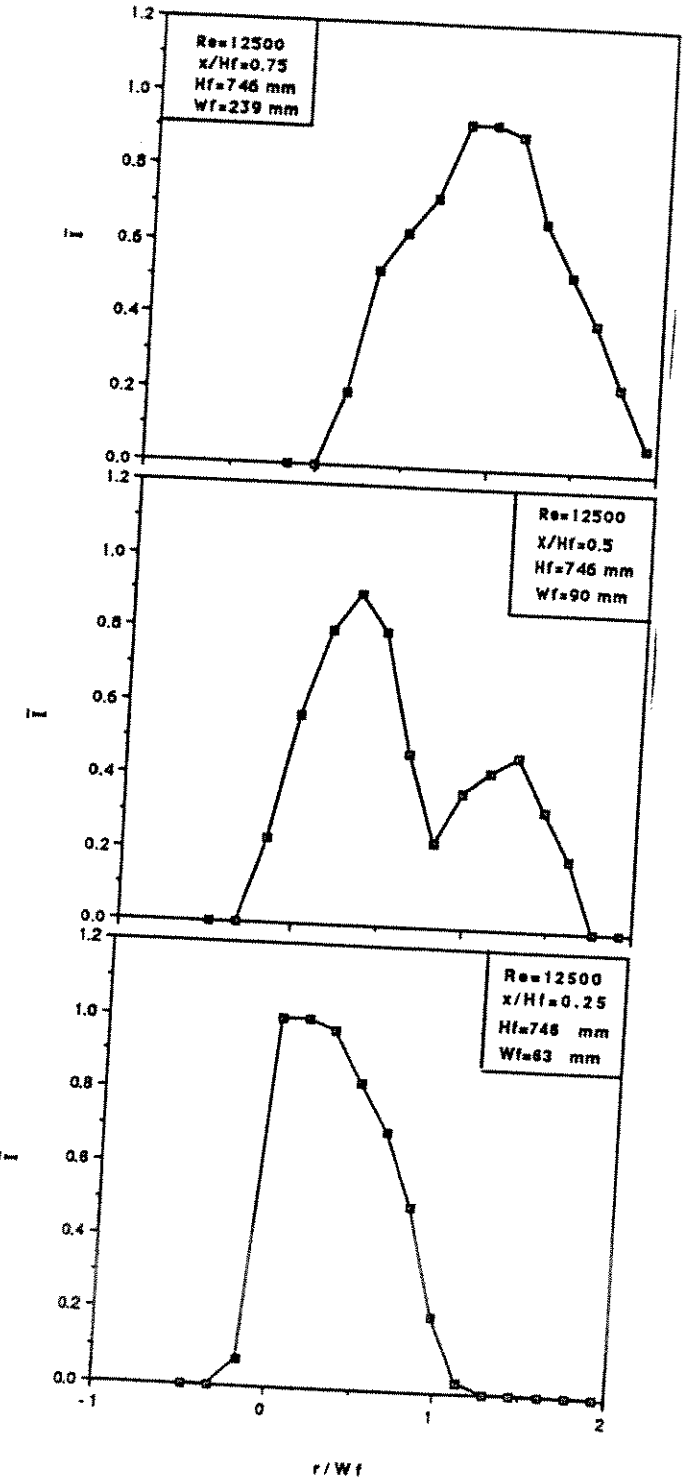

Figure 10. Mean Visible Flame Intermittency, Re = 12500.

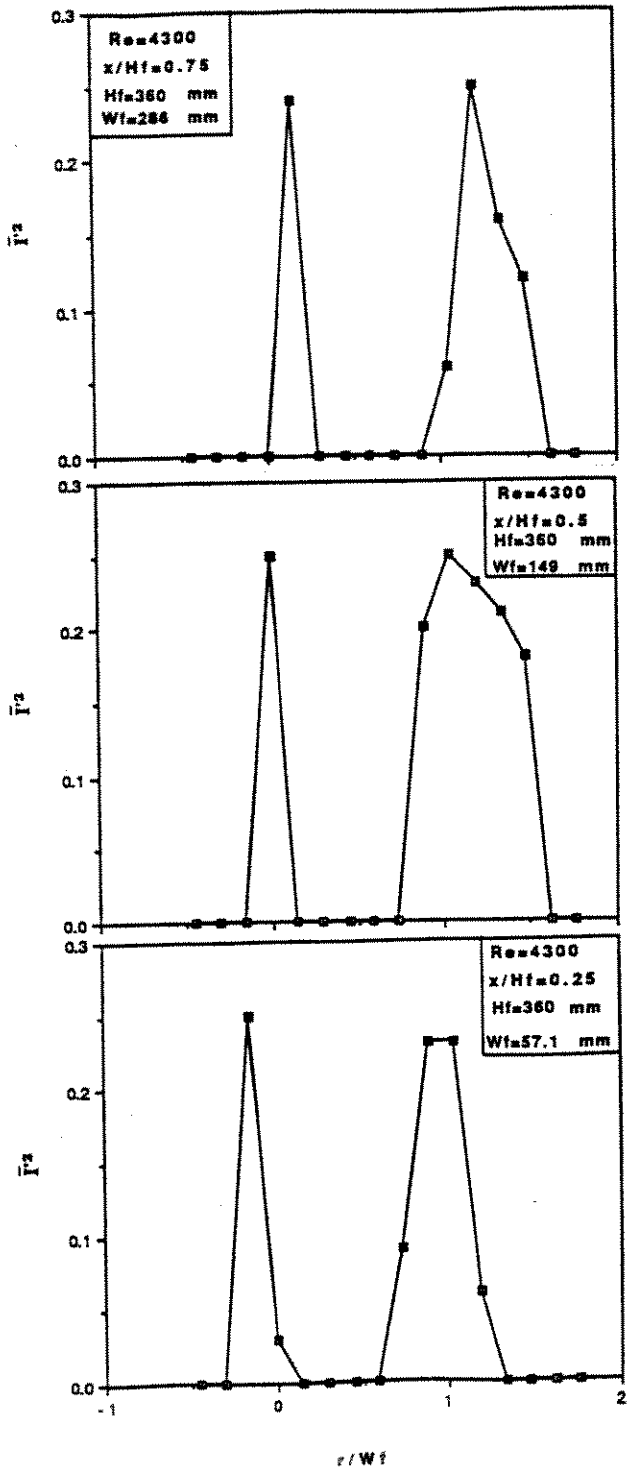

Figure 11. Fluctuating Visible Flame Intermittency, Re = 4300.

The mean square intermittency for the Re=6500 flame plotted in Fig. 12 shows the effects of higher turbulent fluctuations. The lower interface shows less fluctuations as compared to the upper as expected. Two of the lower peaks do not reach the fundamentally correct value of 0.25 only because a calculation at I = 0.5 was not performed. The upper interface shows very broad distribution of flame intermittency caused by buoyant fluctuations.

Figure 13 shows the radial distributions of mean square intermittency for the Re=12500

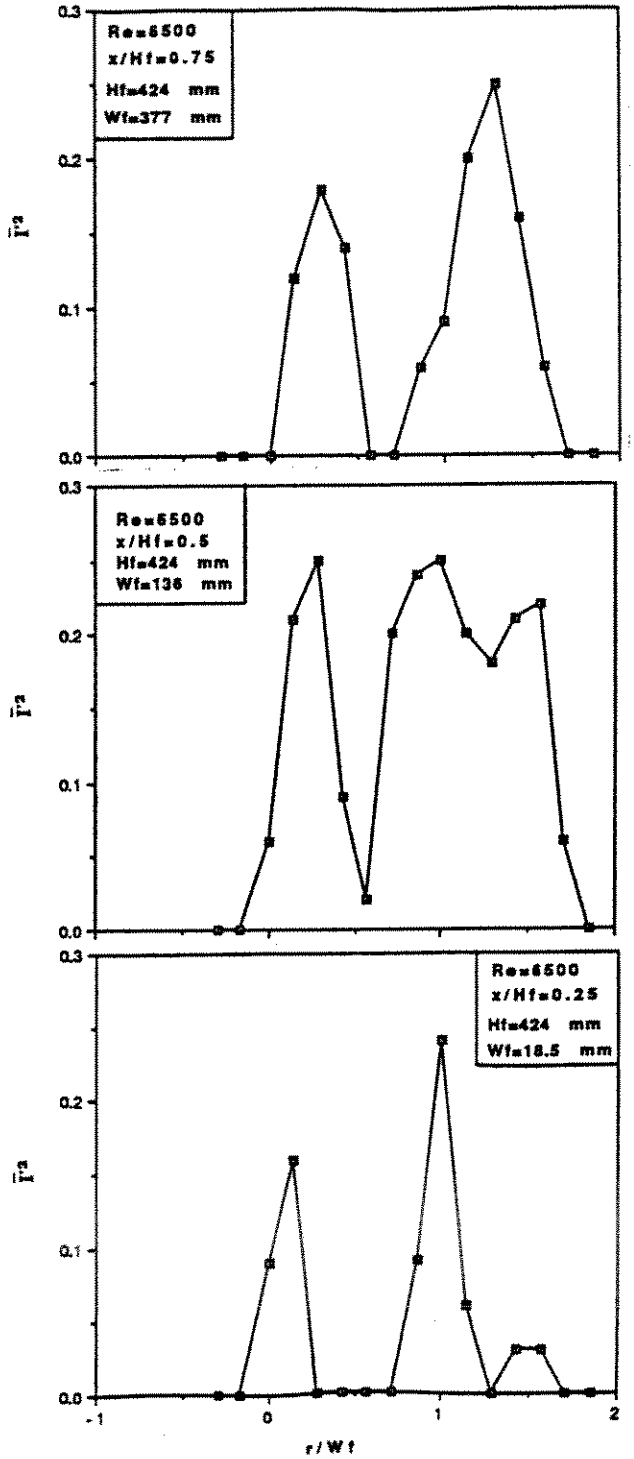

Figure 12. Fluctuating Visible Flame Intermittency, Re = 6500.

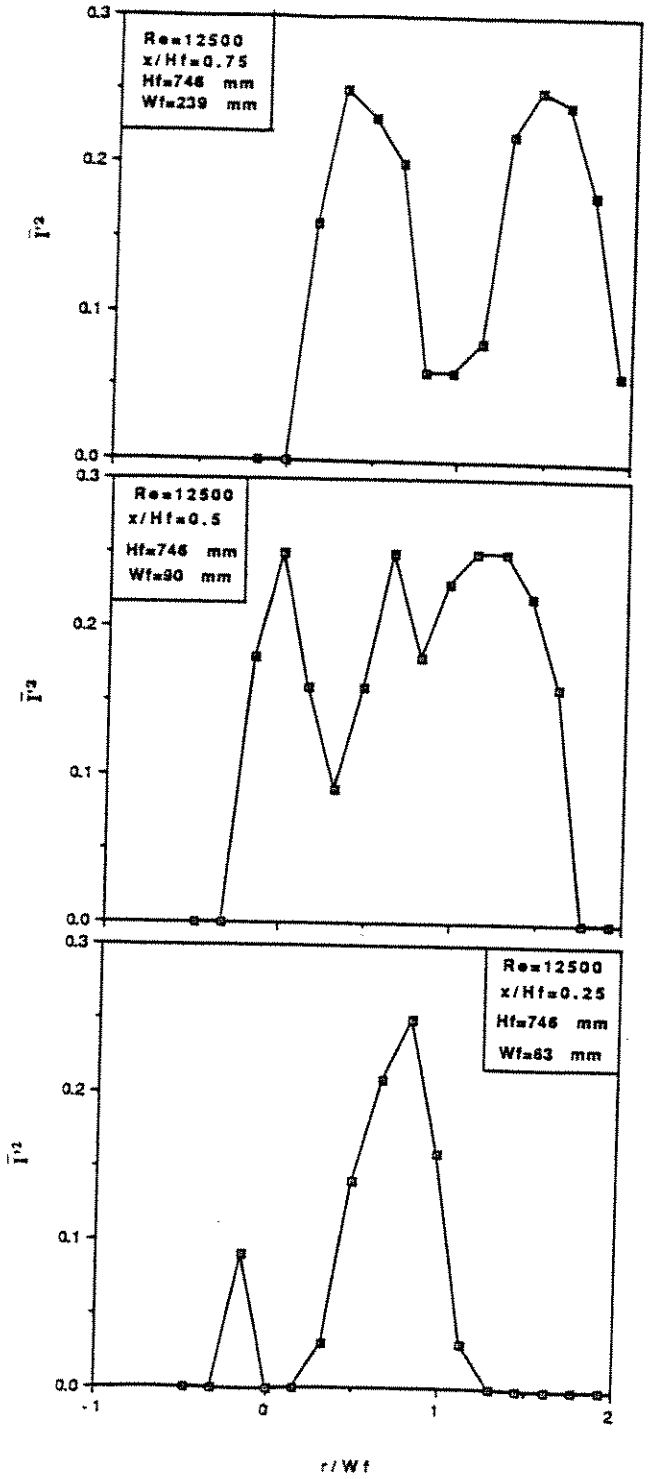

Figure 13. Fluctuating Visible Flame Intermittency, Re = 12500.

flame at three axial positions. Again, a value of 0.25 is not reached at the lowest position since a calculation at a mean intermittency of 0.5 was not performed. The lower interface shows less fluctuations. At x/Hf=0.5, the effects of flames from a downstream position resulting in a much broader distribution and a double peak are observed. At the highest position, both the lower and upper edge show significant flame intermittency. These observations provide direct evidence of buoyancy-turbulence interactions in the present horizontal jet flames.

CONCLUSIONS

Following conclusions can be drawn from the present study:

(1) Trajectories of horizontal flames can be predicted reasonably well using two dimensional finite difference computations in an adaptive coordinate frame.

(2) Transient measurements of flame shapes show significant effects of buoyancy-turbulence interactions. This effect must be considered in modelling the mixing properties of horizontal flames.

ACKNOWLEDGEMENTS

Financial support provided by the Center for Fire Research, National Institute of Standards and Technology under Grant 60NANB8D0834 with Dr. D. D. Evans serving as Scientific Officer is acknowledged. The research program concerning oil well fires at NIST is sponsored by the Mineral Management Service of the Department of Interior with Mr. Ed Tennyson serving as Program Manager.

REFERENCES

Becker H. A., Liang D. and Downey C. I., 1981, Effect of Burner Orientation and Ambient Airflow on Geometry of Turbulent Free Diffusion Flames," Eighteenth Symposium (International) on Combustion, The Combustion Institute, Pittsburgh, PA., pp. 1061- 1071.

Bilger R. W., 1977, "Reaction Rates in Diffusion Flames," Comb. Flame, Vol. 30, pp. 277-284.

Bradshaw P., 1969, "The Analogy between Streamline Curvature and Buoyancy in Turbulent Shear Flows," J. Fluid Mech., Vol. 36, Part 1, pp. 177-191.

Chen C. J. and Singh K., 1990, "Development of a Two-Scale Turbulence Model and Prediction of Buoyant Shear Flows," in Heat Transfer in Turbulent Flow, ASME HTD Vol. 138, R. S. Amano, M. E. Crawford and N. K. Anand, eds., ASME, New York, pp. 53-60.

Chen C. J. and Singh K., 1986, "Prediction of Buoyant Free Shear Flows by k-ε Model Based in Two Turbulence Scale Concept," Proceedings of International Symposium on Buoyant Flows, Athens, Greece, pp. 26-36.

Faeth G. M., Gore J. P., Chuech S. G. and Jeng S. M., 1989, "Radiation from Turbulent Diffusion Flames," Ann. Rev. Numerical Fluid Mech. and Heat Trans., C. L. Tien and T. C. Chawla, eds., Hemisphere, New York, pp. 1-38.

Gore J. P., 1986, "A Theoretical and an

Experimental Study of Turbulent Flame Radiation," Ph. D. Thesis, The Pennsylvania State University, University Park, PA.

Gosman A.D., Lockwood F.C. and Syed S.A., 1977, "Predictions of a Horizontal Free Turbulent Diffusion Flame," Sixteenth Symposium (International) on Combustion, The Combustion Institute, Pittsburgh, PA, pp. 1534-1555.

James R. K. and Edwards D. K., 1977, "Effect of Molecular Gas Radiation on a Planar, Two Dimensional, Turbuelent Diffusion Flame," J. Heat Trans., Vol. 99, pp. 221-226.

Jeng S. M. and Faeth G. M., 1984, "Species Concentrations and Turbulence Properties in Buoyant Methane Diffusion Flames," J. Heat Trans. , Vol. 106, pp. 721-727.

Lamb H., 1945, Hydrodynamics, 6 th ed. 1932, Dover, New York.

Kounalakis M. E., Gore J. P. and Faeth G. M., 1989, "Mean and Fluctuating Radiation Properties of Turbulent Carbon-Monoxide/Air Flames," J. Heat Trans, Vol. 111, pp. 1021-1030.

Launder B. E., 1985, "Progress and Prospects in Phenomenological Turbulence Models," in Theoretical Approaches to Turbulence, Dwoyer D. L., Hussaini M. Y. and Voigt R., eds., Springer Verlag, pp. 155-186.

Madni I. K., 1975, "A Finite Difference Analysis of Turbulent, Axisymmetric, Buoyant Jets and Plumes," Ph. D. Thesis, Iowa State University, Ames, Iowa.

Madni I. K. and Pletcher R. H., 1977, "Buoyant Jets Discharging Nonvertically into a Uniform Quienscent Ambient - A Finite Difference Analysis and Turbulence Modeling," ASME J. Heat Trans., Vol. 99, pp. 641-647.

Pasquill F. and Smith F. B., 1983, Atmospheric Diffusion, Ellis Horwood, John Wiley, New York.

Sinclair J. R., Slawson P. R. and Davidson G. A., 1990, "Three-Dimensional Buoyant Wall Jets Released into Coflowing Turbulent Boundary Layer," ASME J. Heat Trans., Vol. 112, pp. 356-362.

Schlichting H, 1979, Boundary Layer Theory, McGraw Hill, New York, pp. 745-750.

Tamanini F., 1977, "An Improved Version of the k-ϵ-g Model of Turbulence and Its Application to Axisymmetric Forced and Buoyant Jets," Factory Mutual Research, Techn. Rep. 22360-4/RC 77-BT-4.